Investigation on the influence of the target physical properties on an impinging plasma jet

E. Simoncelli[1], A. Stancampiano[1*], M. Boselli[1], V. Colombo[1,2], M. Gherardi[1,2]

[1,2] Alma Mater Studiorum-Università di Bologna, Bologna, Italy
[1]Department of Industrial Engineering (DIN),
[2]Industrial Research Center for Advanced Mechanics and Materials (C.I.R.I.-M.A.M.),
**presently at GREMI, UMR7344 CNRS/Université d'Orléans, Orléans, France*

Abstract: the present works aims at investigating the interaction of plasma with targets with different physical properties. Electrical, morphological and fluid-dynamic characterization was performed on a plasma jet impinging on metal,dielectric and liquid substrates by means of iCCD and high-speed Schlieren imaging techniques. The results highlighted how the light emission of the discharge, its temporal behaviour and morphology and the plasma-induced turbulence in the flow are directly affected by the nature of the target.

Keywords: jet impinging, liquid, metal, dielectric, iCCD imaging, Schlieren imaging, plasma discharge morphology, turbulence.

1. Introduction

The physical and chemical properties of a cold atmospheric plasma jet are not uniquely dependent on the plasma source configuration and operational parameters but also on the target characteristics. The complex mutual interaction between the plasma and the target has recently been the subject of an increasing number of papers investigating various effects of targets on plasma properties such as fluid-dynamics [1–3], electromagnetic field [4,5], reactive and excited species distribution [6], ionization front velocity and propagation [1]. However, these effects can vary dramatically according to the target nature. Especially the electrical properties such as conductivity and potential play a major role [4,7]. During direct plasma treatment the target becomes part of the transient electrical circuit connecting the power supply, the plasma source, the plasma, the target and the connection to ground [8]. Changing the target characteristics will therefor change this circuit and the current and potential drop found in the plasma column. Moreover, in the frame of a wide range of industrial, agricultural and biomedical applications, the interaction of atmospheric plasma jets with liquids is of special interest for the scientific community. Liquid substrates, having both capacitive and conductive components, show a hybrid behaviour between the purely dielectric and purely conductive substrates [1,7]. The present work aims at providing a direct comparison of the behaviour of plasma when interacting with conductive liquid solutions or with a dielectric and metallic substrates, through iCCD and high-speed Schlieren imaging techniques.

2. Materials and Methods

The plasma source adopted in this work is a single electrode plasma jet developed at the Alma Mater Studiorum-Università di Bologna, Italy, and already described, characterized, and applied in a previous work by Colombo et al [1]. The plasma source was driven by a commercial nanosecond pulse generator (FPG 20-1NMK, FID GmbH); the electric conditions used for all the experiments were 15kV as peak voltage (PV) and 125Hz as pulse repetition frequency (PRF). The high-voltage pin electrode (a stainless steel needle; Ø 0.3mm) is centered inside a dielectric channel; a flow rate of 3 slpm of helium gas (99.999% pure) is injected through a 12 holes (Ø 0.3mm) diffuser; the plasma is ejected from the source into the surrounding atmosphere through an orifice with a diameter of 1 mm producing a visible plasma plume interacting with the substrates.

The plasma source was positioned vertically at 10 mm (fixed gap) above the substrate surface.

Different targets were selected for this study, characterized by different conductibility, ranging from metal and liquids to dielectric substrates. A stainless-steel plate (7.6cm×7.6cm×1cm) was chosen as target with infinity conductibility; on the other hand, to simulate a totally-not conductive substrate, a 7.6cm×7.6cm×1cm PVC plate was used as dielectric target. As far as the liquid substrates are concerned, since the electrical conductivity of the target affects the plasma characteristics and in turn plasma treatment may alter the electrical conductivity of the treated liquid solutions, the liquid targets were prepared as phosphate buffer solutions (made dissolving sodium phosphate dibasic (Na_2HPO_4) and potassium phosphate monobasic (KH_2PO_4) in distilled water). Three different solutions characterized by three different electrical conductivities, depending on the concentrations of solutes used, (59 µS, 119 µS and 366 µS with a pH of 7.2) were realized; these physical properties (conductivity and pH) were monitored and maintained unaltered during the experiments. The solution volume was 120 ml contained in a vessel (7.6cm×7.6cm×2cm) with quartz sidewalls and a grounded aluminium bottom.

The morphology and the temporal evolution of the plasma discharge interacting with the substrate were investigated by means of an iCCD camera (Princeton Instruments PIMAX3, spectral response 180–900 nm) equipped with a conventional macro lens (Sigma Dg-Ex-APO-If 180Mm/F3.5, spectral response 380–900 nm). The experimental setup adopted is schematically shown in figure 1. The voltage waveforms were recorded by means of a high voltage probe (Tektronix P6015A) and a current probe (Pearson 6585) connected to an oscilloscope (Tektronix DPO 40034).,The synchronization of the camera gating, driven by the voltage pulses, was performed employing a delay generator (BNC 575 digital pulse/delay generator) and taking into account all possible signal transmission delays as described in [9].

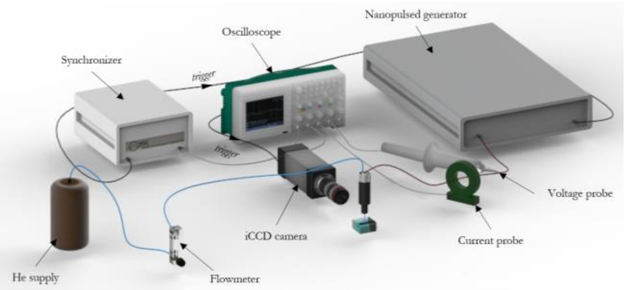

Fig.1 iCCD imaging setup.

The overall intensity produced by the plasma discharge during the main voltage pulse was acquired imposing 35 ns of camera gate exposure, as well as the duration of the voltage pulse. The images were accumulated 30 times with a gain factor set as 50.

The temporal evolution of the plasma discharge during the whole voltage pulse was investigated capturing sequential 10 ns camera gate exposures (each frame results from 30 accumulations. The first iCCD gate opening (0ns) is imposed at the rising of the voltage pulse. The iCCD camera gates are superimposed on the excitation voltage waveforms.

The characterization of the fluid-dynamic behaviour of the discharge was performed using Schlieren imaging technique [10]. The Schlieren setup is shown in figure 2.

It is composed of a 450W ozone free xenon lamp (Newport-Oriel 66355 Simplicity Arc Source) as light source, a slit and an iris diaphragm, two parabolic mirrors with a focal length of 1m, a knife edge positioned vertically to capture horizontal gradients of the refractive index and a highspeed camera (Memrecam GX-3 NAC image technology); the camera was operated at 8000 fps and 1/200000 s shutter time. The plasma source was positioned in the middle of the optical path between the two parabolic mirrors.

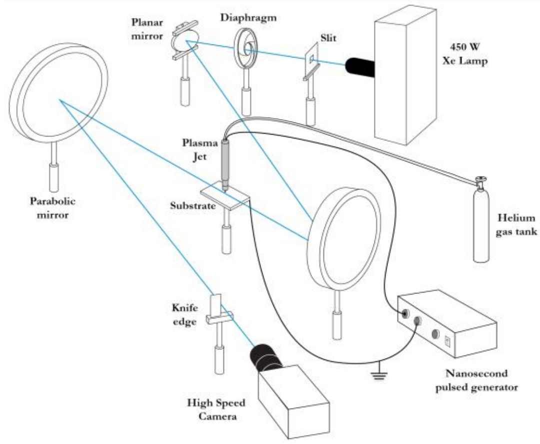

Fig.2 Schlieren high-speed imaging setup.

3. Results and Discussion

In this section, the results for the iCCD imaging of the plasma jet plume impinging on the different substrates, are presented. In Figure 3, for each condition, a single accumulated image of the discharge is shown capturing the light intensity emitted during the whole main voltage pulse (duration of ~35 ns). The acquisitions (Figure 3) highlight how the plasma morphology, and therefore its Vis-NIR light emission, is highly influenced by the nature of the substrate. The strongest intensity and large width of the plasma column are recorded for the case of a metal target. On the other hand, the lowest intensity is observed when the plasma jet is impinging on the liquid substrates; the studied liquid conductivities doesn't seem to relevantly affect the discharge intensity and morphology. Furthermore, a spreading of the plasma over the target surface, known as surface ionization wave (SIW) can be observed mainly in the case of a dielectric substrate and, to a lesser extent, of the metal one. Once the ionization wave impacts the surface, its charging starts to take place and continues for the entire duration of the discharge, inducing a horizontal component of the electric field that favours SIW propagation [4,5].

In Figure 4, the sequence of iCCD images (10 ns exposure) for both dielectric and metal cases are shown. Although it was not possible to precisely evaluate the propagation velocity of the ionization front, the acquisitions in Figure 4 highlight how the temporal evolution of the plasma Vis-NIR light emission is influenced by the nature of the target. For both substrates, the peak of emission intensity is achieved 20 ns after t0, corresponding to the reaching of the maximum applied voltage. In the case of the dielectric target, the images (Fig. 4) show how the Vis-NIR light emission remains approximately constant in time during the whole voltage pulse; differently, when the discharge interacts with the metal substrate, the plasma emission relevantly changes in time: the higher the applied voltage, the higher the light emission.

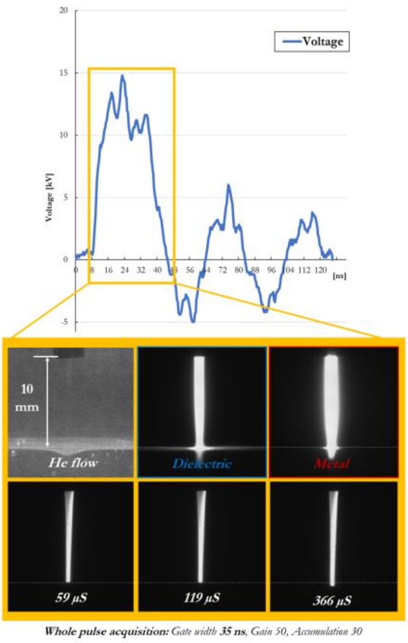

Fig.3 iCCD images related to the whole voltage pulse for all investigated substrates.

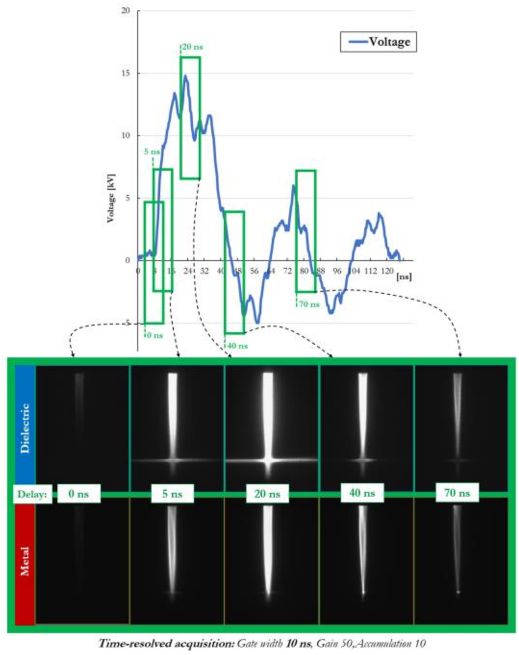

Fig. 4. iCCD images for time-resolved investigation for dielectric and metal substrates.

In Figure 4 the iCCD images reveal how, due to its conductive nature of the metal substrate, the plasma plume does not show a clear SIW formation, but the discharge is focused on a point of the surface. It is worth mentioning that in Figure 3 the images resulted by a time integration of 35 ns, corresponding to the imposed exposure time, and, as shown by the frame 5 ns and 20 ns, some photons are emitted by a surface wider compared to the frames of 40 and 70 ns.

As a matter of fact, in the iCCD time-resolved images, showed in Figure 4, the SIW formation and development are clearly enhanced in the case of plasma jet interacting with the dielectric target due to its higher capacitance. The dielectric surface is charged more than the metallic one, favouring a higher spreading of the plume over the target surface.

Figure 5 presents results for the high-speed Schlieren imaging of the plasma jet plume impinging on the metal, dielectric (top Fig. 5) and liquid (bottom Fig. 5) substrates. The frames are selected with the aim of emphasizing the most important steps of spatial evolution of the turbulent front induced by the discharge: the discharge event, its downstream the axial channel up to 5 mm, its downstream in the axial channel up to 10 mm, its impact with the target surface, its expansion upon the surface.

The duration of the plasma discharge, intended as the ionization front propagation and relative light emission generated by the plasma channel, lasting less than 1 us, is entirely captured in the first frame (0 ms), since the exposure of the high-speed camera is set at 0.005 ms. The time values reported on each frame are indicative of the time lapse between the acquisition of the first frame and the following ones.

In the case of metallic target, a turbulent front is observable at the outlet of the plasma jet since the first image; while for all the other cases, in the first frame (0 ms) the He gas flow results completely laminar, similarly to the case of He gas flow without plasma ignition (data not presented); the He effluent flows out from the source nozzle into open air forming a confined He column along the jet axis. A significant modification of the He flow is evidenced in the following frames, several tens of microsecond after the plasma discharge extinguished. The turbulent phenomenon is thus ignited by the discharge event and its dynamic is directly affected by the nature of target and in turn by the discharge itself.

At 0.25 ms after the onset of the plasma discharge, in all investigated cases, the alteration of the helium flow appears in the form of a transient turbulent structure across the effluent. The turbulent front coming out of the nozzle, propagates downstream with a velocity close to that of the gas flow (~60 m/s). Then, the transient turbulent structure reaches the target surface; several eddies are generated in the gas around the point of impact and progressively move above the surface, departing from the source axis. In all cases, a laminar flow is finally re-established (data not shown) in the He column before the next discharge is generated (8 ms period for PRF 125 Hz).

The strongest turbulent front is observed in the case of metallic substrate and the turbulent structures remain visible more than 5 ms after the discharge event (data not shown). Also for the liquid substrates, the induced turbulent phenomenon is well recognizable, without any relevant differences between the three liquid conductivity investigated. On the other hand, when the plasma jet impinging on a dielectric substrate, the induced turbulence is resulted weaker in comparison to the other studied cases, and the turbulent structures diffusing over the surface interfere with a thin layer of air. Although the onset and the intensity of the discharge induced turbulence are affected by the nature of the target, the timing and dynamic of the front propagation resulted similar among the investigated cases.

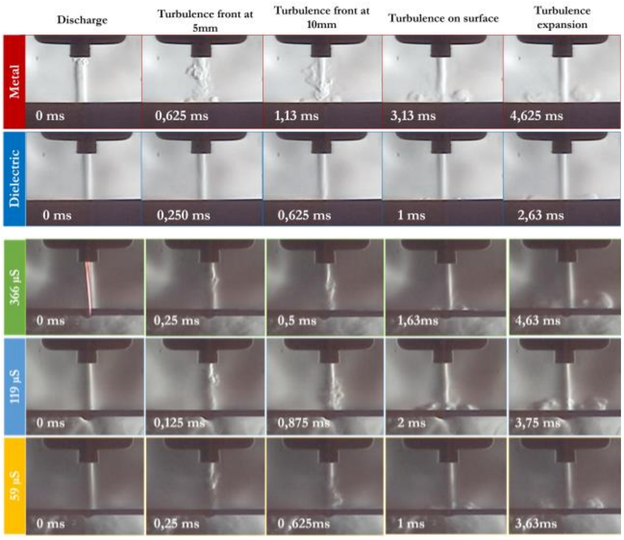

Fig. 5. Schlieren images for metal, dielectric and liquids substrates.

Since before the discharge ignition a laminar flow is always re-established, we can assume that the turbulence is a consequence of the discharge. At the ignition of the plasma, a sufficient strong and local modification of the physical and thermal properties of the He flow occurs resulting into the onset of a turbulent front.

Based on the considerations reported by Bruggeman *et al.* [13] for similar APPJ configurations, we can link the formation of turbulent structures to an increase in gas temperature, that in turn leads to a decrease of gas density and to an increase in gas velocity. According to this explanation, the magnitude of the alteration should be proportional to the amount of heat released by the high-voltage electrode. Therefore, the strongest turbulent front is observed in the case of plasma interacting with the metallic substrate: since the substrates are grounded, electric field and the current density should be maximized in the case of target with the highest conductibility, represented by the metallic substrate in this work.

Finally, the gas impinging on the liquid substrates causes the formation of an axisymmetric cavity, a dimple, on the surface. The effects of impingement of a gas jet on a liquid surface have been studied in different scientific and industrial fields [14]. As described in [1], the impact of the turbulent front upon the liquid surface causes a variation of the dimension of the dimple in time.

4. Conclusions

The present study highlights, through an ICCD and Schlieren imaging analysis, how the plasma plume changes its morphology and its light intensity as a consequence of the physical properties of the target, and how the fluid-dynamic of the plasma-induced turbulent front is affected by the substrate's nature. This work could be considered as a new step in the understanding of the complex interaction of non-equilibrium plasma with a substrate.

5. References

[1] A. Stancampiano, E. Simoncelli, M. Boselli, V. Colombo, and M. Gherardi, Plasma Sources Science and Technology 16 (2018).

[2] M. Boselli, V. Colombo, E. Ghedini, M. Gherardi, R. Laurita, a. Liguori, P. Sanibondi, and a. Stancampiano, Plasma Chemistry and Plasma Processing **34**, 853 (2014).

[3] E. Robert, V. Sarron, D. Riès, S. Dozias, M. Vandamme, and J.-M. Pouvesle, Plasma Sources Science and Technology **21**, 034017 (2012).

[4] T. Darny, J.-M. Pouvesle, J. Fontane, L. Joly, S. Dozias, and E. Robert, Plasma Sources Science and Technology **26**, 11 (2017).

[5] O. Guaitella and a Sobota, Journal of Physics D: Applied Physics **48**, 255202 (2015).

[6] K. Gazeli, G. Bauville, M. Fleury, P. Jeanney, O. Neveu, S. Pasquiers, and J. Santos Sousa, Plasma Sources Science and Technology **27**, (2018).

[7] Y. Yuanfu, P. Xuekai, G. Dogan, W. Fan, W. Shuqun, L. Xinpei, Y. Yue, X. Pei, D. Gidon, and F. Wu, Plasma Sources Science and Technology **27**, 11 (2018).

[8] F. Judée, J. Vaquero, S. Guégan, L. Fouassier, and T. Doufour, J. Phys. D: Appl. Phys 0 (2019).

[9] M. Gherardi, N. Puač, D. Marić, A. Stancampiano, G. Malović, V. Colombo, and Z. L. Petrović, Plasma Sources Science and Technology **24**, 064004 (2015).

[10] E. Traldi, M. Boselli, E. Simoncelli, A. Stancampiano, M. Gherardi, V. Colombo, and G. S. Settles, EPJ Techniques and Instrumentation **5**, 23 (2018).

[11] S. Norberg, Modeling Atmospheric Pressure Plasma Jets: Plasma Dynamics,Interaction with Surfaces, Liquid Layers and Cells, University of Michigan, 2015.

[12] S. A. Norberg, E. Johnsen, and M. J. Kushner, Journal of Applied Physics **118**, 013301 (2015).

[13] S. Zhang, A. Sobota, E. M. van Veldhuizen, and P. J. Bruggeman, Journal of Physics D: Applied Physics **48**, 015203 (2015).

[14] F. R. Cheslak, J. A. Nicholls, and M. Sichel, Journal of Fluid Mechanics **36**, 55 (1969).